J Mater Sci (2008) 43:3832–3836
DOI 10.1007/s10853-007-2218-1

In-situ observations of a martensitic transformation in a Cu–Zn–Al single crystal driven by stress or strain

Erell Bonnot · Ricardo Romero · Michel Morin · Eduard Vives · Lluís Mañosa · Antoni Planes

Received: 19 July 2007 / Accepted: 10 October 2007 / Published online: 3 April 2008

Abstract We have studied the stress–strain hysteresis loops during the martensitic transition of a Cu–Zn–Al single crystal. The transition was mechanically induced either under stress-driven or strain-driven conditions. The comparison between the two mechanisms shows significant differences in the transformation path. In situ optical observations in strain-driven experiments reveal retransformation which results in a re-entrant behaviour. No re-entrancy is found in stress-driven experiments. The hysteresis is larger in stress-driven experiments.

Introduction

Martensitic transformations are first-order diffusionless structural transitions among crystalline phases [1]. A single crystal of the high temperature phase splits into a number of twin-related variants due to spontaneous symmetry breaking. These variants configure a complex heterostructure (or polyvariant structure). The presence of an externally applied (directional) field breaks this degeneracy thus resulting in a reduced number of favourable variants. In shape-memory materials, this occurs when the transition is mechanically induced at constant temperature by controlling either the applied force (stress) or the displacement (strain). These two particular control variables are conjugated variables in the thermodynamic sense. For a macroscopic system in equilibrium, thermodynamic trajectories should not depend on the control variable since force and conjugated displacement are related by a Legendre transformation [2]. However, martensitic transitions do not occur in equilibrium and therefore differences in strain- and stress-driven trajectories may exist. It is expected that these differences should be enhanced when the transition dynamics has an athermal character [3]. In this case, thermal fluctuations do not play a relevant role and non-equilibrium is a consequence of the existence of high-energy barriers that can be overcome only by driving the system to a marginal stability situation from which it can relax to a metastable configuration.

In the present work, we present experiments performed on a Cu–Zn–Al shape-memory crystal under both force and displacement control conditions. This material undergoes a martensitic transition from a cubic to a monoclinic structure which is known to take place in almost ideally athermal conditions when the transition is thermal-induced [4]. Usually, stress–strain experiments are undertaken using commercial tensile testing machines in which the control variable is elongation (related to strain). In order to perform stress-driven experiments, we have developed an experimental device which enables fine control of the applied force while the strain is monitored. Results will provide a meaningful comparison of stress–strain trajectories under both driving conditions. The work is aimed at

E. Bonnot (✉) · E. Vives · L. Mañosa · A. Planes
Departament d'Estructura i Constituents de la Matèria, Facultat de Física, Universitat de Barcelona, Diagonal 647, Barcelona 08028, Catalonia (Spain)
e-mail: erell@ecm.ub.es

R. Romero
IFIMAT, Universidad del Centro de la Provincia de Buenos Aires, Pinto 399, 7000 Tandil, Argentina

R. Romero
Comisión de Investigaciones Científicas de la Provincia de Buenos Aires, 7000 Tandil, Argentina

M. Morin
Groupe d'Etudes de Métallurgie Physique et Physique des Matériaux, INSA de Lyon. 20, Av. A. Einstein, 69621 Villeurbanne, France

finding out possible differences in the trajectories from specific features of the interface motion in the two cases.

Thermodynamics

It is interesting to revise the concept of equilibrium and metastable states in order to better understand the experimental results presented in the following sections. Equilibrium states correspond to minima of a thermodynamic potential, such as the elastic-free energy $\Phi(X)$, defined on the set $\Omega = \{X\}$ of available states of the system. Assume that a constraint imposed by an external device keeps, for instance, the length (strain) fixed in a certain direction. This represents a condition that can be expressed as $S(X) = s$, which restricts the set of available states for minimization. For this constrained minimization problem, we obtain a set of solutions $\{X^c(s)\}$ which are the minima of Φ for selected values of s. Let us now consider a closely related, but different minimization problem for which a new potential (Gibbs elastic energy) $\Gamma(X) = \Phi(X) - \sigma S(X)$, is defined. σ is a new thermodynamic variable which has dimensions of stress. Minimization of the new potential over Ω without any constraint renders a set of solutions $\{X^u(\sigma)\}$ parameterized by the stress σ. The question to be addressed is, under which conditions are the two sets of solutions $\{X^c(s)\}$ and $\{X^u(\sigma)\}$ identical and, in this case, which is the relationship between s and σ? From a mathematical point of view, this question has a well-defined answer when the function $\Phi(s) = \Phi[X(s)]$ is convex. In this case, it can be shown [5] that the two sets $\{X^c(s)\}$ and $\{X^c(\sigma)\}$ are equivalent. Namely, for each value of the constraint s a value of σ exists such that $X(s) = X(\sigma)$. Moreover, it can be shown that σ and s are related through the derivative $\sigma = \partial\Phi(s)/\partial s$. Note that this is equivalent to stating that Γ is a Legendre transform of Φ. The above scenario is the standard situation in equilibrium thermodynamics, illustrated in Fig. 1a. This situation also applies for equilibrium first-order phase transitions. In this case the function $\Phi(s)$ is flat in the transition region [as illustrated in Fig. 1b] because any free-energy barrier between the parent and product phases vanishes in the thermodynamic limit. The existence of the flat region gives rise to a value of stress σ for which there is a degeneration of states $X^u(\sigma)$. These are the inhomogeneous states corresponding to s values located within the coexistence region.

In this work, we deal with first-order phase transitions which take place out of equilibrium in athermal conditions (thermal fluctuations do not promote the transition). Energy barriers are very high and therefore the system cannot find absolute minima, instead it remains in local metastable minima until limits of metastability are reached (barriers disappear) by changing an external field. In this case, the evolution of the system is determined by a potential that exhibits concave regions, as illustrated in Fig. 1c. In these regions, the equivalence of the constrained and unconstrained problem does not hold and different trajectories for systems driven by either controlling the external stress or the strain are expected. Indeed, recent theoretical approaches based on the random field Ising model [6] have revealed different behaviour for the two situations.

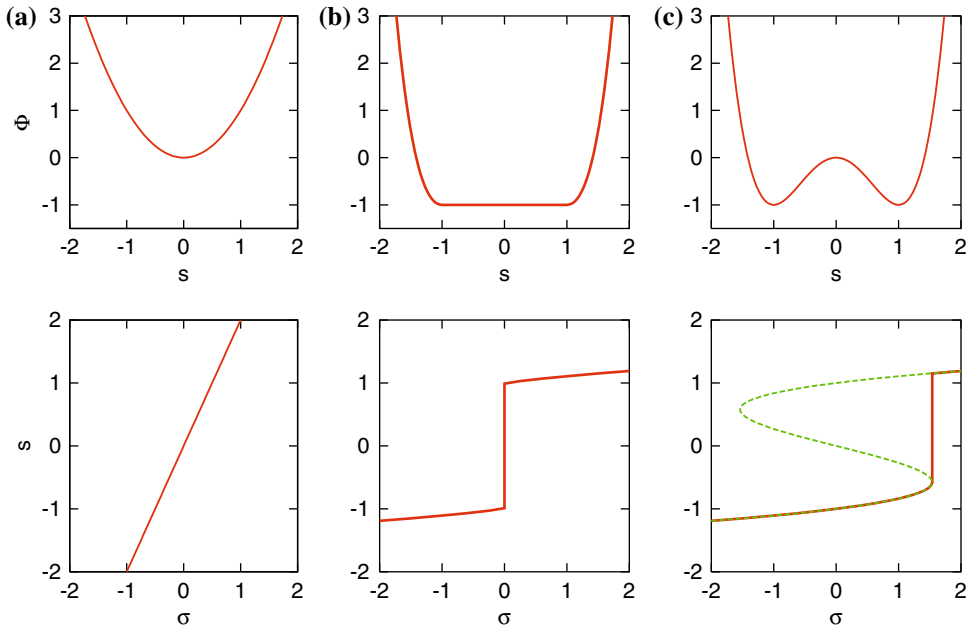

Fig. 1 Schematic examples of the behaviour of the functional $\Phi(s)$ (above) and the corresponding evolution of the strain s versus the stress defined as $\sigma = \partial\Phi/\partial s$. (**a**) corresponds to a standard equilibrium point, (**b**) to an equilibrium first-order phase transition and (**c**) to an athermal transition. In the latter case, the continuous line shows the athermal behaviour for the stress-driven case. The system in this case follows an intermediate trajectory between the dashed and continuous lines

Experimental details

A single crystal of Cu–Zn–Al, obtained by melting metals of 99.999% purity, was grown by the Bridgman method. The composition of the crystal was determined from EDX to be $Cu_{68.13}Zn_{15.74}Al_{16.13}$. The crystal undergoes an athermal martensitic transition on cooling from a $L2_1$ cubic to a monoclinic (18R) structure at $T_M = 234$ K. A rectangular sample with cylindrical heads was machined from the ingot. The body of the sample has flat faces 35 mm long, 3.95 mm wide and 1.4 mm thick. The crystallographic direction of the tensile axis is close to the [001] direction of the cubic phase. The sample was annealed at 1,073 K for 30 min, cooled down to room temperature in air and finally aged for 2 h in boiling water. This heat treatment ensures that the sample is in the ordered state, free from internal stresses and that the vacancy concentration is close to the equilibrium case. The flat surfaces of the sample were mechanically polished to allow in situ microscopic observations during the experiments. These flat surfaces were determined to be oriented parallel to the (520) planes by means of texture X-ray diffraction.

Experiments were carried out using two different experimental devices as represented in the insets of Figs. 2 and 3. The first device (strain-driven) is a commercial INSTRON 4302 tensile machine which allows control of the elongation while the load is monitored. The second device (stress-driven) has been especially designed to enable fine control of the load while the elongation is monitored. These two devices use the same special grips, designed to adapt the cylindrical heads of the sample. A thorough description of these devices can be found in [7]. In addition, in order to perform in situ microscopic observations and monitor the interface motion, an optical microscope with a CCD camera can be adapted at room temperature and fitted to both devices.

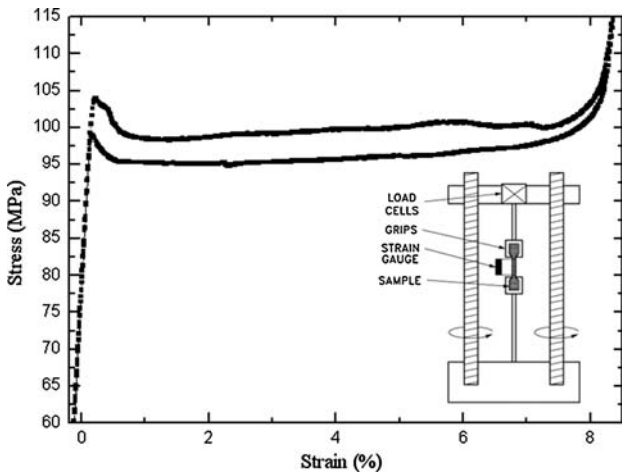

Fig. 2 Stress–strain curves obtained in the strain-driven case, at $T = 295.4$ K with an elongation rate of $v = 0.005$ mm/s. The inset shows a scheme of the INSTRON machine used to perform this experiment

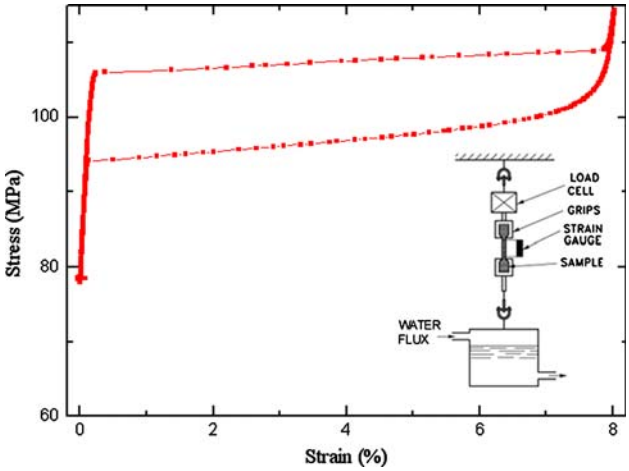

Fig. 3 Stress–strain curves in the stress-driven case at $T = 294.2$ K, at a loading rate of $v = 0.467$ N/s. The inset shows a scheme of the mechanical device designed to perform this experiment

Results

Figure 2 shows a typical example of stress–strain curves recorded in strain-driven experiments. Upon loading, the cubic phase elastically deforms until it becomes unstable and the martensitic transformation starts. A relaxation of the stress (yield point effect) is observed just after the start of the MT. At higher strain values, the stress weakly oscillates around an almost constant value as the MT progresses. After completion of the transition, the martensite is elastically deformed. Upon unloading, the same re-entrant behaviour causes the yield point at the end of the reverse transformation. It is worth noticing that the existence of a yield point has already been reported in similar experiments in MT [8, 9].

Different behaviour [illustrated in Fig. 3] is observed for the stress-driven experiments: the hysteresis is significantly larger than in the strain-driven experiments and no yield point is observed. As MT proceeds, the stress slightly increases with an average slope which increases with rate. The positive slope is due to a rate of propagation of the interface lower than the externally imposed rate. The smaller dissipation in the strain-driven case can be understood taking into account that the displacement is constrained but the force is able to relax to lower values in such a way that the system can follow a trajectory that approaches equilibrium.

We have studied whether or not the transition under stress or strain driven conditions shows athermal character.

This has been done by analyzing its dependence on stress or strain rate, following the scaling procedure explained in [10]. Results indicate that for the onset of the transformation, the behaviour is athermal whereas for later stages deviations have been detected. They have been attributed to kinetic effects associated with latent heat dissipation.

Optical observations were performed in situ for the two sets of experiments. In the two cases, several martensitic plates nucleate [see Figs. 4a, 5a]. The plates correspond to the same single martensitic variant which propagates towards the ends of the specimen as the transformation proceeds [Figs. 4d, 5d]. We have applied the crystallographic theory for MT [11] in order to elucidate what the observed martensitic variant is. From the 24 symmetry-allowed variants for a cubic to monoclinic martensite, the one with the highest Schmidt factor is favoured in tensile experiments. There are two shear systems with high Schmidt factor, which can be easily activated by a tensile stress applied close to the [001] direction. These systems are indicated in the stereographic projection shown in Fig. 6 where P1 and P2 stand for the habit planes and d1 and d2, for the corresponding shearing directions. The angles between these directions and the tensile axes are 74° and 38° for d1 and d2, respectively. The angle observed experimentally is approximately 75° which confirms that the selected variant is d1. This result agrees with crystallographic theory since this shear system has the highest Schmidt factor.

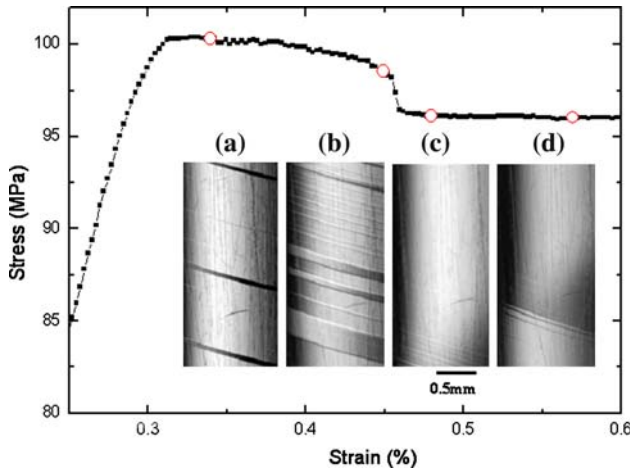

Fig. 4 Micrographs of the microstructure observed during a strain-driven experiment at $T = 294.2$ K and $v = 0.005$ mm/s for different strain values (indicated by open circles): (**a**) 0.34%, (**b**) 0.45%, (**c**) 0.48% and (**d**) 0.57% strain

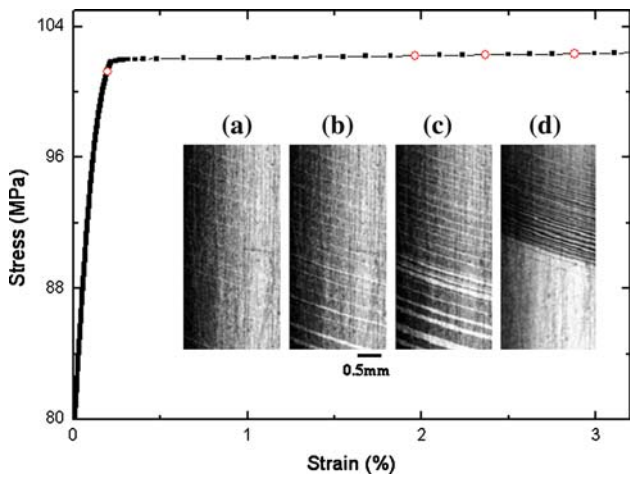

Fig. 5 Micrographs of the microstructure obtained during the stress-driven experiment at $T = 295.5$ K and $v = 0.137$ N/s for different stress values (indicated by open circles): (**a**) 101.25 MPa, (**b**) 102.22 MPa, (**c**) 102.28 MPa, (**d**) 102.34 MPa

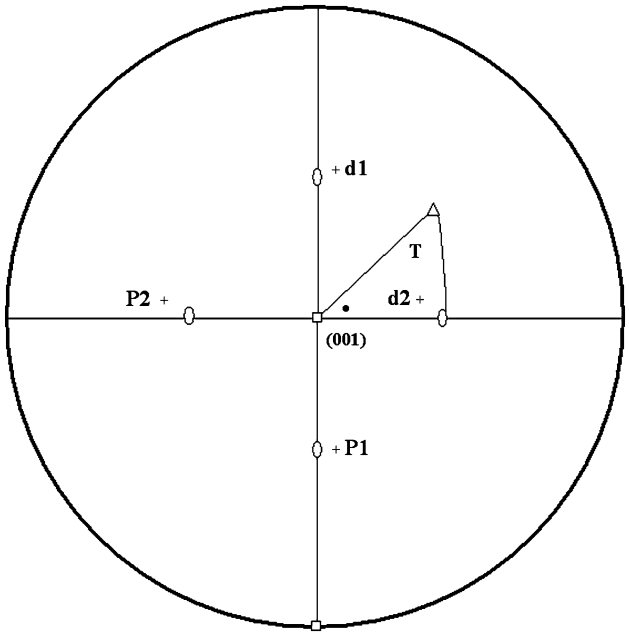

Fig. 6 Stereographic projection of the cubic phase. T is the fundamental triangle for the tensile axis, P1, P2 are the habit planes and d1, d2 the shear directions corresponding to the variants of the 18R structure with higher Schmidt factor. The solid circle indicates the direction of the tensile axis

Specific analysis of the early stages of the MT reveals significant differences between the two driving mechanisms. Figures 4 and 5 show the upper branch of the stress-strain curves in the strain-driven and stress-driven cases along with the micrographs obtained at fixed values of the control parameter. In the strain-driven case, the comparison between pictures (Fig. 4) obtained at different strain values shows that a certain amount of the martensitic phase transforms back to the cubic phase (retransformation). This explains that the yield point effect arises from the shrinkage and eventually the disappearance of previously formed martensitic plates. On the other hand, in the stress-driven case, there is a deviation of pure elastic behaviour below the yield stress. This effect is due to a nucleation of very

thin martensitic plates all over the sample, as illustrated in Fig. 5a. In this case, as the system is free to accommodate the deformation, nucleation can be observed at lower load values.

Conclusion

We have carried out an experimental study of systems undergoing first-order phase transitions with athermal characteristics with different constraints in the control variable. Martensitic transitions offer a unique scenario for this study since they can be induced either by controlling the strain (constrained case) or the stress (unconstrained case). We have shown that the trajectories in the constrained case are different from those in the unconstrained one. In particular, when the control variable is the strain, the stress–strain curves exhibit a yield point effect and lower dissipation. Optical observations have revealed that the yield point arises from the retransformation of part of the material.

Acknowledgements This work has received financial support from CICyT (Spain), project MAT2007-61200, CIRIT (Catalonia) project 2005SGR00969, and Marie Curie RTN MULTIMAT (EU) contract MRTN-CT 2004-5052226.

References

1. Bhattacharya K (2003) Microstructure of martensite Oxford Series on Materials Modelling. Oxford University Press, Oxford
2. Huang K (1987) Statistical mechanics, 2nd edn. John Wiley and Sons, New York
3. Ortín J, Planes A, Delaey L (2005) In: Mayergoyz I, Bertotti G (eds) The Science of Hysteresis. vol 3, Elsevier, p 467
4. Pérez-Reche FJ, Vives E, Mañosa L, Planes A (2001) Phys Rev Lett 87:195701
5. Costeniuc M, Ellis RS, Touchette H, Turkington B (2005) J Stat Phys 119:1283
6. Illa X, Rosinberg ML, Vives E (2006) Phys Rev B 74:224403; Illa X, Rosinberg ML, Shukla P, Vives E (2006) Phys Rev B 74:224404
7. Bonnot E, Romero R, Illa X, Mañosa L, Planes A, Vives E (2007) Phys Rev B 76:064105
8. Landa M, Novák V, Sedlák P, Sittner P (2004) Ultrasonics 42:519
9. Iadolica MA, Shaw JA (2004) Int J Plast 20:577
10. Planes A, Perez-Reche FJ, Vives E, Mañosa Ll (2004) Scr Mater 50:181
11. Otsuka K, Wayman CM (1998) Shape memory materials. Cambridge University Press, Cambridge